TOPICAL ISSUE ARTICLE

Fuel inventory and material migration of JET main chamber plasma facing components compared over three operational periods

View the article online for updates and enhancements.

Fuel inventory and material migration of JET main chamber plasma facing components compared over three operational periods

A Widdowson[1,10] , **S Aleiferis**[2] , **E Alves**[3] , **L Avotina**[1,4] ,
A Baron-Wiechec[1,5] , **N Catarino**[3] , **J P Coad**[1], **V Corregidor**[3] ,
K Heinola[6,7] , **I Jepu**[8] , **C Makepeace**[1,9] **and JET Contributors**[11]

[1] Culham Centre for Fusion Energy, Culham Science Centre, Abingdon, OX14 3DB, United Kingdom
[2] Institute of Nuclear and Radiological Sciences and Technology, Energy and Safety, National Center for Scientific Research 'Demokritos', Athens, 15310, Greece
[3] IPFN, Instituto Superior Técnico, Universidade de Lisboa, 1049-001, Lisboa, Portugal
[4] University of Latvia, Institute of Chemical Physics, Riga, Latvia
[5] Guangdong Technion—Israel Institute of Technology, Shantou, 515063, People's Republic of China
[6] International Atomic Energy Agency, Vienna International Centre, PO Box 100, A-1400 Vienna, Austria
[7] University of Helsinki, PO Box 64, FI00560 Helsinki, Finland
[8] National Institute for Laser, Plasma and Radiation Physics, 077125, Romania
[9] Department of Materials, University of Oxford, Parks Road, OX1 3PH, United Kingdom

E-mail: anna.widdowson@ukaea.uk

Abstract

Fuel retention and material migration results from JET ITER-like wall beryllium limiter tiles are presented for three operating periods. Ion beam analysis results support the general picture of erosion during limiter configurations with local deposition on tile ends far into the scrape off layer. Similar trends of fuel concentrations are observed in all JET operating periods; (i) low on surfaces exposed to high heat flux and erosion and (ii) higher in deposits. The pattern of fuel retention and deposition correlates with heat flux and distribution of limiter plasmas touching inner and outer limiters. The D/Be ratio in the thickest deposit is ~0.01. Global fuel retention attributed to limiters is <0.01% of injected fuel. Marker coatings reveal a rapid transition from strong erosion to deposition within 15 mm. This work highlights the need to carefully consider the requirements of marker coatings for long exposure studies in high erosion areas.

Keywords: fuel retention, material migration, beryllium, erosion, deposition, JET ITER-like wall

(Some figures may appear in colour only in the online journal)

1. Introduction

The JET tokamak is currently operating with the wall materials to be used in ITER; beryllium in the main chamber and tungsten in the divertor. The operation of the JET ITER-like (JET-ILW) wall has allowed for plasma facing materials to be studied by *post mortem* analysis to understand erosion, deposition, material migration and fuel retention for ITER relevant materials, one of the prime objectives for the overall JET-ILW project [1]. In this paper data for beryllium (Be) main chamber tiles spanning the three operating periods of the JET-ILW are presented, giving the most comprehensive picture of fuel retention and material migration poloidally around the main chamber. The results summarise data obtained from a nine year programme of ion beam analysis of Be main chamber limiter and upper dump plate (DP) tiles. Previous *post mortem* analysis of JET Be tiles have reported erosion

---

and deposition results for tiles exposed 2011–12 (ILW1) [2], fuel retention in limiter tiles (ILW1) [3], (2013–14 (ILW2)) [4, 5], erosion features (ILW1) [6] and castellation gaps (ILW1) [7].

2. Experimental details

The surfaces of Be limiter and upper DP tiles removed from JET after each operating period have been studied at the ion beam facility based at IPFN, Instituto Superior Técnico. The following ion beam analysis techniques have been used; elastic back scattering (EBS) using 2.3 MeV H^+, nuclear reaction analysis (NRA) using 2.3 MeV $^3He^+$ reactions, $^9Be(^3He, p)^{11}Be$, $^{12}C(^3He, p)^{14}N$, $^2H(^3He, p)^4He$, and particle induced x-ray emission (PIXE). The scattering angle for the EBS detector and PIXE detector is $150°$. For the NRA detector the scattering angle is $135°$. The cross sections measured for the system are $^9Be(^3He, p)^{11}B$ [8] and $^9Be(p, p, 0)^9Be$ [9]. In addition the cross sections used are $C(^3He, p)^{14}N$ [10] and calculated $D(^3He, p)^4He$ and $D(^3He, ^4He)p$ following the methods of [11]. Further details of the detectors used may be found in [12]. At this facility the large vacuum chamber with glove box attached enables whole JET tile samples contaminated with Be and tritium (T) to be handled.

For the JET-ILW operations spanning three operating periods, a total of thirty-six bulk Be tiles have been removed for analysis from inner limiter (IL), outer limiter (OL) and DP locations. The poloidal distribution of the tiles removed are indicated by shading in figure 1. Of the tiles removed twenty-nine tiles have been analysed by ion beam methods, indicated by ✓/∼ in table 1. A subset of these tiles was equipped with marker coatings of composition Be 7–8 μm/Ni 2–3 μm/Be bulk. The tiles with marker coatings are indicated by shading in table 1. The aim of using marker coatings is to enable erosion rates to be determined from the change in thickness of the coating. To achieve this the following design constraints need to be met: (i) the coating must be sufficiently thin for measurement by IBA at available beam energies, in this case 2.3 MeV H^+, (ii) the coating must be thick enough that if total erosion of the layer occurs the erosion can be determined by other means (e.g. surface profiling), and (iii) the interlayer should have similar thermal expansion properties to avoid stress and delamination as a result of cyclic heating. These factors were considered in the development and testing of the marker coatings for Be tiles [13, 14]. The marker coating experiment ran mainly during ILW1 and ILW2 operating periods.

The analysis of IBA data has been completed using the code IBA DataFurnace (NDF) [15] which enables simultaneous EBS, NRA and PIXE data to be processed to provide concentration depth profiles and integrated atomic concentrations over the analyses depths, as described in [12]. At the beam energy used the maximum interaction depth for the deuterium (D) concentration analysis from $^3He^+$ NRA is 9 μm. For the tungsten (W) and nickel (Ni) quantification the maximum interaction depth is 10 μm for H^+ in Be.
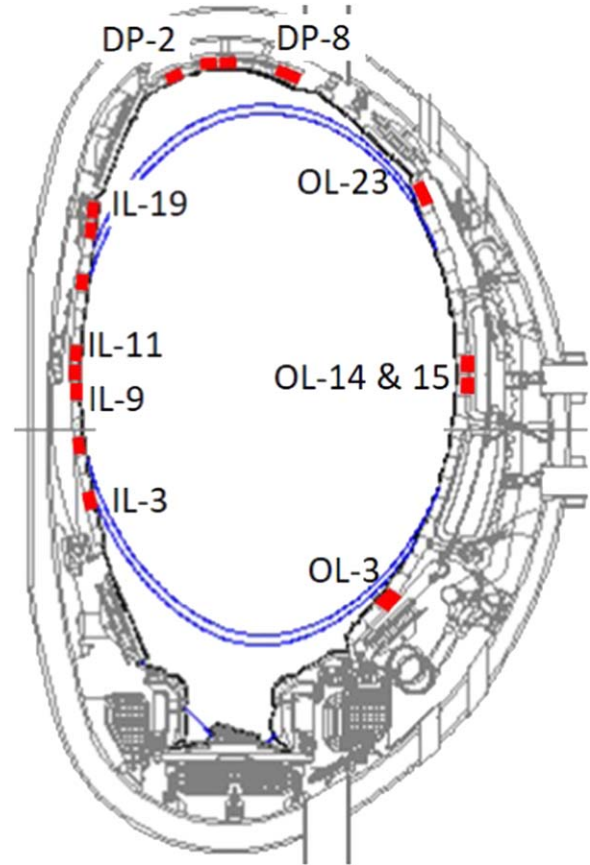

Figure 1. Cross section of JET with the poloidal location of beryllium tiles removed indicated.

In section 4 the global fuel retention data are presented for main chamber Be tiles. The results rely on interpolation between the analysed tiles in the poloidal direction along limiter beams and multiplying by the number of limiter beams toroidally around the vessel. A second order polynomial has been used for the interpolation along the limiters. In some cases, the IL beams are only partially populated with bulk Be tiles, with the remaining tiles being recessed. In these cases, only the bulk Be tiles are considered in the extrapolation; the recessed tiles are not included in the calculation.

3. Results

3.1. Fuel retention

The fuel retention for IL, OL and DP tiles are shown in figures 2–4 respectively. For the first time D concentrations remaining in Be main chamber tiles from the bottom to the top of the IL and OL and from high field to low field ends of the DP beams are shown with results from all three operating periods. In general the distribution of fuel toroidally across a tile shows similar trends for all of the JET operating periods; that is (i) low fuel concentrations in the central part of the mid-plane limiter tiles (IL10/11 figure 2(c), OL14/15 figure 3(b)) where there is high heat flux and erosion and (ii) higher fuel concentrations at the ends of the tiles where there

Table 1. Details of bulk beryllium main chamber tiles removed from JET for analysis. Note all tiles were newly installed in 2011 for the JET-ILW configuration. ✓ = IBA data, ∼ = IBA data to be processed, ✗ = no IBA data, → = tile not removed from vessel after operating period specified in column heading and therefore exposed for more than one operating period. Grey shading indicates tiles with marker coating Be 7–8 μm/Ni 2–3 μm/Be tile.

	ILW1 (2011–12)	ILW2 (2013–14)	ILW3 (2015–16)
Inner limiter tiles (IL)			
IL19	✓	✓	∼
IL18	✗	→	✗
IL15	→	✓	∼
IL11	→	→	✓
IL10	✓	✓	✓
IL9	✗	→	✗
IL6	→	✓	∼
IL3	✓	✓	∼
Outer limiter tiles (OL)			
OL23	✓	✗	✗
OL15	→	→	✓
OL14	✓	✓	✓
OL3	✓	✓	∼
Dump plate (DP)			
DP2	✓	✓	✓
DP4	∼	✓	✓
DP5	→	→	✓
DP8	→	→	✓

is deposition. The fuel desorption characteristics for OL14 and IL10 are discussed in an accompanying paper in these proceedings [16].

The retention on IL tiles above (IL15) and below (IL6 and IL3) the mid-plane shows an asymmetric retention pattern. There is higher fuel concentration on the left side (−80 to 0 mm) of IL15 above the mid-plane and on the right side (0–80 mm) of IL6 below the mid-plane, with low fuel concentration on the opposite side of the centre line of the tiles. At the very top of the IL fuel retention on IL19 is uniform in comparison to the mid-plane section.

The highest fuel concentration for all Be limiter tiles is observed on the OL14 after ILW1, generally reaching $2–3 \times 10^{18}$ D atoms cm^{-2}, with a few higher values recorded, figure 3(b). In fact, fuel concentrations on the ends of OL tiles are either comparable or higher than for the IL tiles. Similar trends are found in [16, 17].

Evidence for lower D retention in divertor tiles and limiter tiles after ILW2 when compared with ILW1 has been reported. This is linked with the ILW2 operating period ending with ∼300 pulses in hydrogen (H) [5, 18, 19]. In these results the effects are mainly associated with regions where deposition occurs. This is due to co-deposition with H instead of D, and probable removal of pre-existing D in deposits by isotope exchange. For the IL10 tile there is lower D concentration following ILW2 on the right-hand (RH) end when compared with ILW1 data. However, the effect is not seen on the left-hand (LH) end of the same tile. For the lower IL3 and
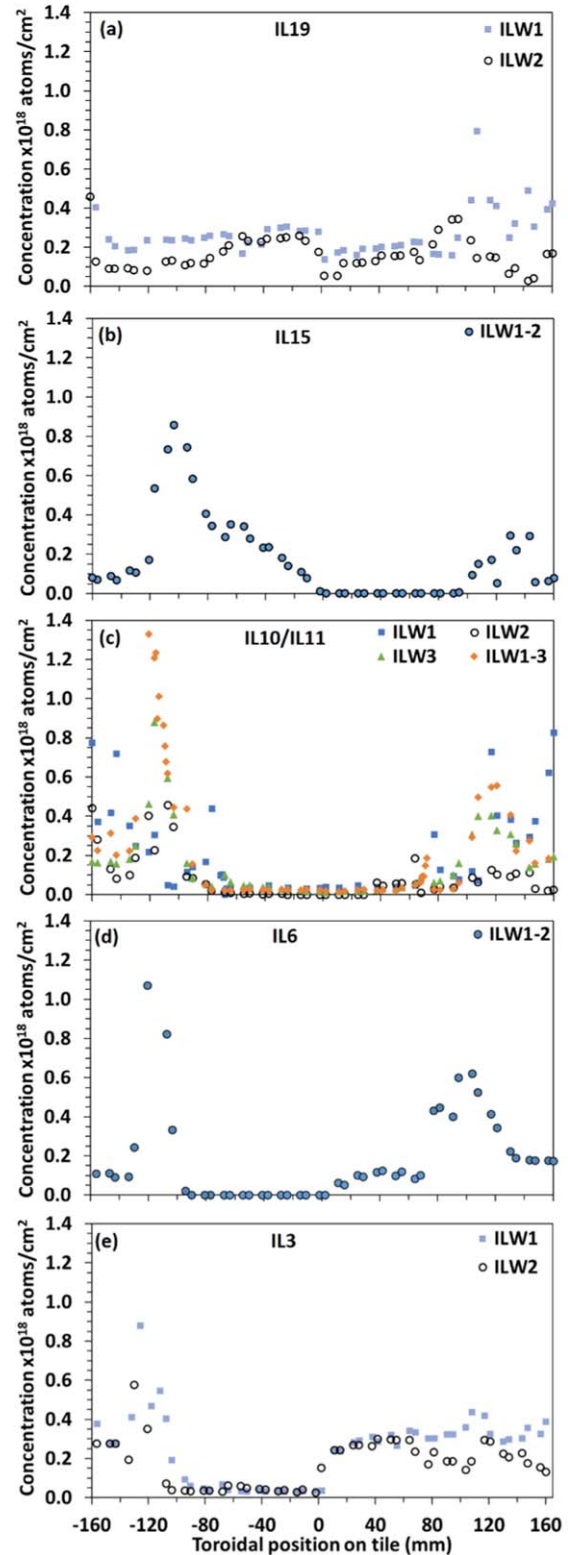

Figure 2. Deuterium areal concentration in inner limiter (IL) tiles. (a) IL19 at top of limiter after ILW1 and ILW2, (b) IL15 after ILW1-2, (c) IL10 at mid-plane after ILW1 [18], ILW2 (data reproduced with permission of copyright holder UKAEA and author) [18] and ILW3, and IL11 after ILW1-3, (d) IL6 after ILW1-2, (e) IL3 at bottom of limiter after ILW1 and after ILW2. 0 mm is the centre of the tile, negative values are on the left and positive values are on the right of the tile when viewed facing the inner wall.
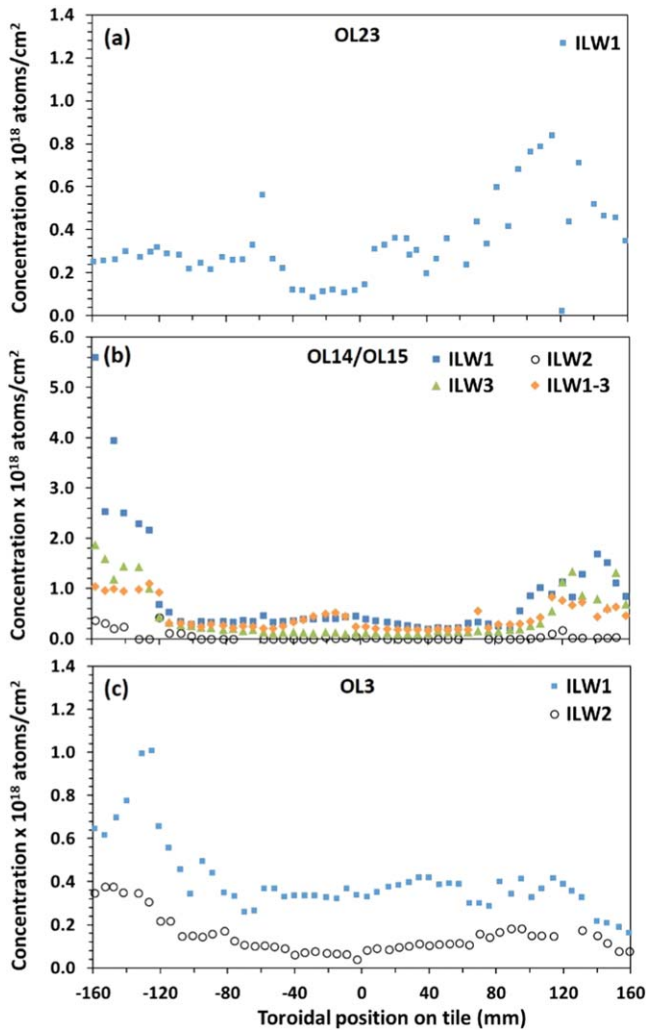
Figure 3. Deuterium areal concentration in outer limiter (OL) tiles. (a) OL23 at top of vessel after ILW1, (b) OL14 at mid-plane of vessel after ILW1 (Data set reproduced with permission from EURATOM) [3], ILW2 (Data set reproduced with permission from Elsevier) [5] and ILW3, and OL15 after ILW1-3 (note change in scale for concentration), (c) OL3 at bottom of limiter after ILW1 and ILW2. 0 mm is the centre of the tile, negative values are on the left and positive values are on the right of the tile when viewed facing the outer wall.

Figure 4. Deuterium areal concentration on dump plate (DP) tiles. (a) DP2 after ILW1, ILW2 and ILW3, (b) DP4 after ILW2, ILW3 and DP5 after ILW1-3. 0 mm is the centre of the tile. Positive values are to the right of the tile and negative values to the left of the tile, when following a poloidal line from the inner wall up to the dump plates.

upper IL19 tiles there is only a small difference between ILW1 and ILW2 seen mainly on the RH end of the tiles. The most significant change in D concentration is seen at the lower OL3 and mid-plane OL14 tiles, where clear reductions are seen after ILW2 when compared with ILW1. In regions of high heat flux, fuel retention is already low and therefore conclusions about the influence of H are not possible.

For the dump plate tiles DP2 and DP4, figure 4 (a) and (b), the D concentrations on the surface exposed to ion current (−45 to 0 mm) are lower than on the surface shadowed from the ion current (0–45 mm) where a small amount of deposition occurs. DP8 (results in [20]) was subject to strong interaction with plasma during vertical displacement events (most of which occurred during ILW2) resulting in melting. Despite the periodic heating above the melting temperature
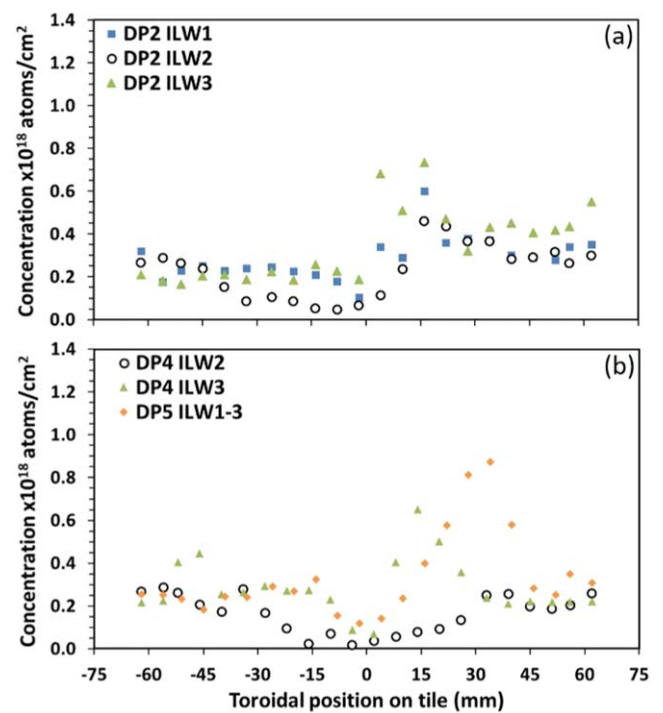
the fuel retention across DP8 (0.2–0.4 $\times 10^{18}$ atoms cm^{-2} [20]) is higher than the high heat flux regions on the limiter tiles and is similar to the levels to DP2 and DP4. Lower D values are seen for ILW2 on DP4 after H plasmas, figure 4(a). The effect is not so pronounced for DP2, figure 4(b).

When comparing fuel concentrations for tiles exposed for each of ILW1, ILW2 and ILW3 with the tile exposed for all three campaigns ILW1-3 there are some variations. For the IL11, although there is a significant peak in the fuel concentration on the LH side of the tile, on the RH side there is no major difference in fuel concentration for the tile exposed for three operating periods. The discrepancy in the integrated deuterium concentration may be due to the thickness of the deposit exceeding the analysis depth by IBA. Electron microscopy of samples show 5 μm deposits at −130 to −134 mm on the LH side of IL10 (after ILW1), figure 5, and ∼10 μm deposits on the RH side [21]. Similar results are seen when comparing OL14 with OL 15. For the OL15 exposed for ILW1-3 the fuel concentration is similar to that for tile OL14 exposed for ILW3 only. Electron microscopy shows layered deposits that exceed 10 μm on OL14 in the region −152 to −158 mm (not shown). Therefore after three operating periods a thickness greater than 9 μm, i.e. the maximum analysis depth for D, could be expected in the regions of highest deposition and consequently the D concentration in deposits for tiles exposed ILW1-3 shown in figures 2 and 3 may not give the full integrated result. For OL14 (after ILW3) and OL15 (after ILW1-3) one could speculate that the tile exposed for three campaigns shows an overall lower
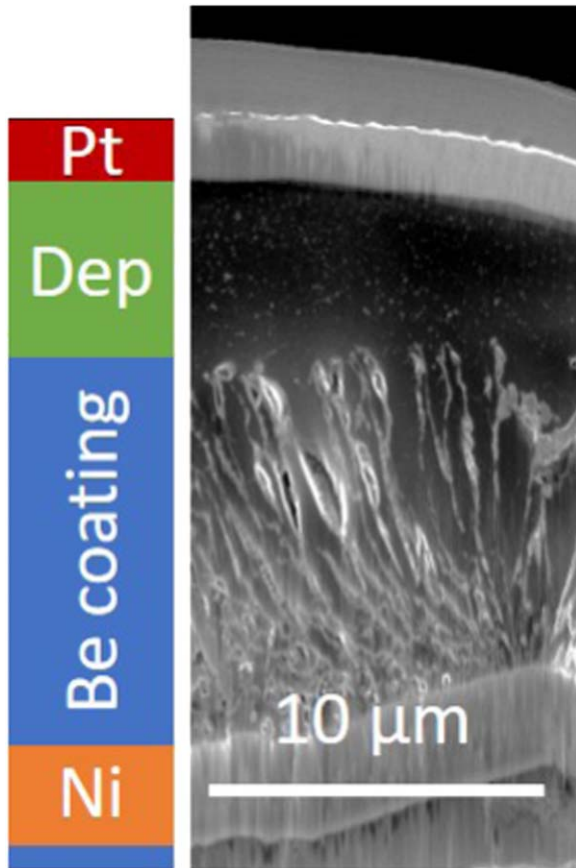
Figure 5. Micrograph of IL10 in the region −130 to −134 mm. Be/Ni marker coating are intact with deposited layer on top. The light-coloured layers at the top for the micrograph are platinum deposited during the processing by focused ion beam milling. The layer above this is the extent of the platinum surface in three-dimensions.

concentration as the analysis incorporates the lower D concentration from the ILW2 operating period. Alternatively, it may also be that deposition is not cumulative over long periods; there may be limits to deposit thickness due to geometric, thermal influences or adhesive properties of the deposits.

3.2. Erosion and deposition, material migration

Following exposure in JET, the marker coatings were completely removed from the central regions of the IL10 and OL14, whilst on the ends of the tiles the marker coatings were covered by deposit. At the bottom and top of the limiters the coatings remained intact with no appreciable erosion. There are generally only 2–3 data points spanning a 10–15 mm band in the transition from erosion to deposition zones that show partial erosion. Even for IL6 below the mid-plane with erosion on the left side (−80 to 0 mm) of the tile and deposition on the right side (0–80 mm), there is just one point to the right of the centre line (at 5 mm) that clearly shows partial erosion of the marker coating. Thus, the erosion experiment using marker coatings has shown that there is a rapid transition from strong erosion (marker layers removed) to deposition along the tile. This could be indicative of the decay in ion densities

and/or energies beyond the separatrix of the limiter plasma. However due to the rapid change, no conclusive data on net Be erosion rates during limiter plasmas was obtained using this method.

In order to map material erosion, migration and deposition in JET one can introduce an isotope or dissimilar element not usually found in the vessel, which can be detected by analysis techniques. One such study tracks the migration of ^{10}Be isotope from a mid-plane IL tile enriched by neutron irradiation [22, 23]. An alternative approach is to look at the mid and high atomic number (Z) impurities seen in the deposited layer to establish the deposition pattern. In JET the common mid and high-Z impurities are Ni, iron (Fe) and chromium (Cr) which derive from erosion of the Inconel® outer vessel wall by charge exchange neutrals (CXNs) and also W coming from main chamber and divertor tile erosion [24]. Indeed Ni and W are seen on the surfaces of all limiter tiles around the vessel at low concentrations $\sim 10^{17}$ atoms cm^{-2} [2].

The quantification of Ni, Fe, Cr and W relies on PIXE analysis in combination with EBS. A complicating factor for the quantification of Ni is that the interlayer in the marker coating is Ni. This prevents a simple integral value for Ni being reported from the IBA data for ILW1 and ILW2 tiles. For these tiles it is necessary for each analysis point to be studied to deconvolute the surface Ni peak from the integral value. This type of study was completed for ILW1 [24] but has not yet been completed for ILW2. It is also feasible to study Cr and Fe concentrations since it has been shown that deposited Ni, Cr and Fe are always in the correct ratio for Inconel® [24], however this data is not presented here. Instead, the Ni and W concentrations for OP14 after ILW3 and OP15 after ILW1-3, and IL10 after ILW3 and IL11 after ILW1-3, i.e. tiles without marker coatings, are shown in figure 6. Results for W concentration for ILW1, ILW2 and ILW3 can be found in [24]. For the OP tiles the LH side shows similar concentrations of Ni and W for ILW3 and ILW1-3, whereas on the RH side the data is less consistent (figure 6(a)). For the IL limiter tiles a more consistent picture shows that deposition for ILW1-3 is greater than for ILW3, whereas concentrations on the RH side are similar by comparison (figure 6(b)). Whilst the effect of overall thickness might account for much of these differences as discussed in section 3.1, one also has to consider that the rate of the W and Ni sources may vary within and between operating periods.

Another method for studying migration is to introduce gases into the vessel, such as nitrogen (N$_2$). With the tiles available there is a possibility to study N deposition by EBS. Although a full assessment of N has not been completed there is evidence of N on the limiter tiles. For example, on IL15 exposed for ILW3, N is co-deposited on the LH side of tile (−77 mm from the centre line) in a narrow band at a concentration of 3.7×10^{17} atoms cm^{-2}. The number of N atoms injected into JET during ILW3 was 2.3×10^{24}, two orders of magnitude lower than the number of D atoms (see table 2). As N$_2$ is injected into the divertor, either into the scrape off layer or private flux region depending on the location of the strike points, this demonstrates a migration path from the divertor to
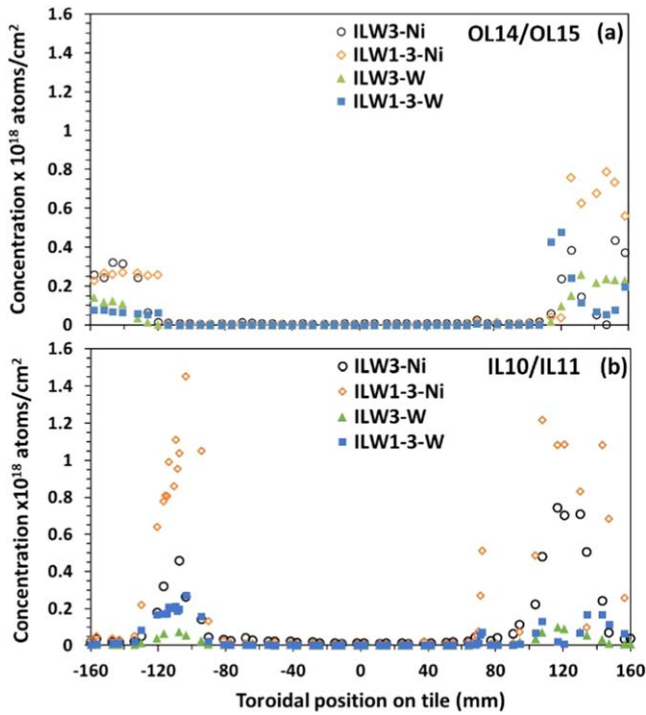
Figure 6. Nickel and tungsten deposition on (a) mid-plane outer limiter tiles OL14 (after ILW3) and OL15 (after ILW1-3) and (b) mid-plane inner limiter tiles IL10 (after ILW3) (data reproduced under CC BY NC ND) [24] and IL11 (after ILW1-3). The toroidal position along the tile is as described in figure 3 for OL tiles for (a) and as described in figure 2 for IL tiles for (b).

Table 2. Fuel retention in Be limiter and dump plate tiles. D atoms injected for fuelling from gas introduction modules (GIMS) and total D atoms injected including via neutral beams and pellets.

	ILW1	ILW2	ILW3
D atoms injected (GIM)	2.6×10^{26}	2.6×10^{26}	2.2×10^{26}
Total D atoms injected[a]	9.1×10^{26}	5.8×10^{26}	6.4×10^{26}
Inner limiter	1.4×10^{22b}	0.8×10^{22}	1.2×10^{22}
Outer limiter	5.2×10^{22b}	0.8×10^{22}	3.2×10^{22}
Dump plate	1.2×10^{22}	0.9×10^{22}	1.6×10^{22}
Total D in Be tiles	7.8×10^{22}	2.5×10^{22}	6.0×10^{22}
Limiter plasma time (h)	6	5.2	4.9
Divertor plasma time (h)	13	14.2	18.5

[a] Gas injected from disruption mitigation valve not included. Global fuelretention calculated using values in the shaded columns.
[b] Retention values after Heinola *et al* [4].

the inner wall. Further work to elucidate N_2 migration is needed.

4. Discussion

The fuel retention, erosion and deposition on limiter tiles are influenced predominantly by direct plasma interaction during limiter phases which results in a heat flux profile. An example of the heat flux for one pulse during ILW1 at the IL is shown in [25] where it can be seen that the highest heat flux is at the
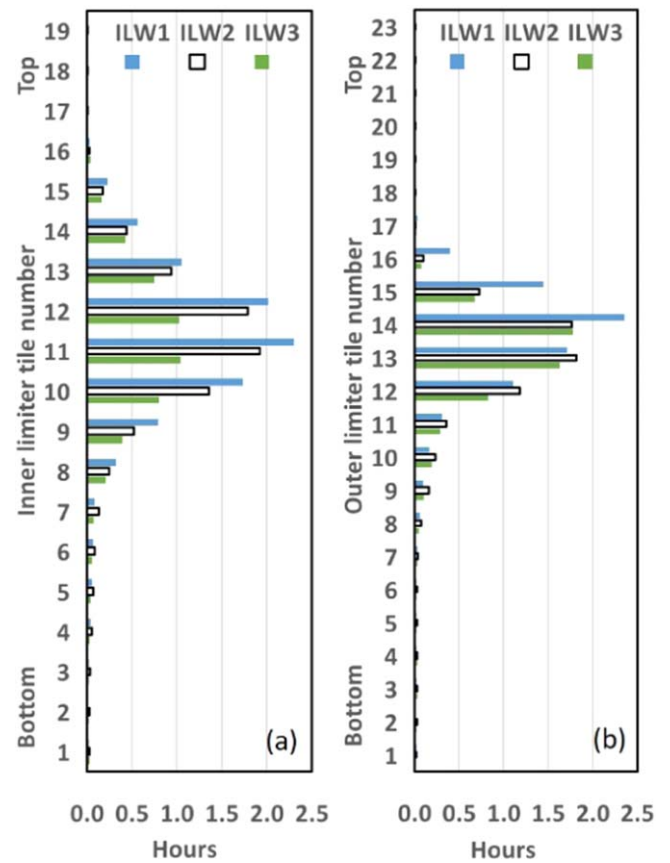

Figure 7. Distribution showing time of limiter plasma within 2 mm of (a) inner or (b) outer limiter surfaces.

centre of the mid-plane IL tiles, and to the RH side above the mid-plane and to the LH side for IL tiles below the mid-plane. Even though the IBA data from the Be limiter tiles shows the average over an operating period, the fuel retention results from the IL show a clear relationship of low fuel retention where highest heat flux occurs. Although a full integration of heat flux data from IR camera images over the whole operating period is not possible as it would require significant resource, it is possible to show the distribution of plasma touching the limiters, see figure 7. It is clear that the main interaction occurs at the midplane tiles. When examining the plasma contact time, we see that for ILW1 there was more contact time on IL10 than for ILW3, probably due to Be erosion studies in limiter configuration [26]. This was reflected in the relative W concentrations seen in deposits on the LH side (−107 mm); 1.7:1.3:0.7 h limiter time compared with 140:125:60 × 10^{15} W atoms cm^{-2} [24] for ILW1:ILW2: ILW3 respectively. On the RH side however, the correlation of deposition with limiter time was not observed. The W source is predominantly due to erosion in the divertor during divertor plasmas and material migration in the scrape off layer. Therefore, this result suggests some deposition on limiters during divertor configurations and subsequent erosion and local re-deposition onto the ends of limiter tiles in limiter plasmas in accordance with the erosion/deposition processes discussed below.

Further work to investigate limiter conditions such as temperature and energy deposited onto tiles is underway but not sufficiently developed to present here.

Global fuel retention in Be limiters and the upper dump plate has been previously reported for ILW1 [3, 4], however the work presented here is the most complete analysis of all Be limiter and DP tiles available. The results are shown in table 2. Fuel retention values for the ILW1 IL and OL Be tiles are quoted from [4]. However, for ILW1 the DP retention value is recalculated. In [4] the ILW1 DP retention was calculated based on the result of one tile, DP2, with no trends along the DP ridge available. The new calculation follows the same trends in D concentration now seen for ILW2 and ILW3 taking into account results from two tiles DP2 and DP4, i.e. a decrease in D concentration at the tile surface from the high field side towards the low field side of the DP ridge. This calculation gives a lower retention value for DP retention for ILW1 than previously reported [4]. In addition, the global retention data for ILW2 and ILW3 is newly calculated. The limiters and upper dump plate account for $\sim 0.01\%$ of total fuel injected into JET, with the OL having a higher inventory than the IL tiles in ILW1 and ILW3. The interpolation for ILW3 OL tiles follows the same curve as for ILW1, as the D results for OL3 and OL 23 are not currently available. Although the calculation for the total fuel inventory makes several assumptions it is still worth noting that the individual OL14 mid-plane tile shows higher fuel inventory than IL10 mid-plane tile, and furthermore the OLs make up a larger surface area, with 16 OLs compared with 10 ILs. Overall lower global D retention values are lower for ILW2 due to ending the JET experimental operations with 300 pulses of hydrogen (H) plasmas as discussed in section 3.1.

To date the global fuel retention including the divertor and recessed areas for ILW2 and ILW3 has not been calculated, however the fraction of the global retention attributed to the IL, OL and DP Be tiles after ILW1 was in the range 20%–25% [4]. Limiter plasmas contribute 25%–30% of the total plasma operation time in JET. High effective Be sputtering yields are also observed in limiter plasmas (in comparison to divertor plasmas) with the eroded material predominantly deposited in the main chamber [26]. This implies that net retention rates due to co-deposition on limiters during limiter plasmas is comparable with net retention rates on divertor tiles and plasma remote surfaces during divertor plasmas. Additional erosion of limiters by CXNs during divertor plasmas does not significantly change the net deposition as only a fraction of eroded material is redeposited locally; the majority migrates to the upper inner divertor [26, 27]. Furthermore, the Be erosion rate due to CXNs, 5.5×10^{13} atoms cm^{-2} s^{-1} [28], results in a total erosion of $\sim 3 \times 10^{18}$ atoms cm^{-2} during divertor plasmas. This is $\leqslant 5\%$ of the 5–10 μm deposits on Be limiters which are equivalent to 0.6–1.24 $\times 10^{20}$ atoms cm^{-2}.

In general D/Be ratios have not been reported as detailed analysis is required at each point to determine the thickness of Be deposits on a Be substrate. However, an estimate of D/Be ratio due to co-deposition can be calculated from the thick deposits for IL11 (after ILW1-3). The D concentration in deposits is 1.4×10^{18} atoms cm^{-2} in the maximum 9 μm interaction depth of 1.12×10^{20} atoms cm^{-2}, giving a ratio of ~ 0.01. In terms of mass this is $\sim 0.2 \times 10^{-2}$ g D/g Be deposit. Assuming a similar retention fraction for T plasmas this would equate to 0.3×10^{-2} g T g^{-1} Be deposit, giving an upper limit from co-deposition equivalent to 1×10^{12} Bq g^{-1} Be deposit, where the specific activity of T is 357×10^{12} Bq g^{-1} T [29].

5. Summary and conclusions

Fuel retention, erosion, deposition and material migration data are presented for all JET-ILW campaigns. The results show that for tiles exposed for entire operating periods a global pattern is established with most erosion taking place at the mid-plane IL and OL tiles. Eroded material is deposited onto the ends of limiter tiles, where most fuel is retained by co-deposition. The D/Be ratio is ~ 0.01 in the thickest deposits seen on IL11 and OL15 exposed for all three operating periods. Global fuel (D) retention on the limiters for ILW1 and ILW3 are $\sim 0.01\%$, and lower for ILW2 which ended with H plasmas. Fuel retention rates on the limiters are of a similar order to retention rates for the remaining inventory in the divertor and on remote surfaces.

The Be erosion study using marker coatings was of limited success on JET limiter tiles. It was found that the surfaces of the limiter tiles were either strongly eroded, in which case the marker coating was removed, or strongly deposited in which case the marker coating was covered. There were only limited bands 10–15 mm across tiles where partial erosion of the marker coating was observed, indicative of the decay in ion density and/or energy beyond the limiter plasma separatrix. This is in contrast to erosion studies at the recessed inner wall where lower Be erosion rates due to CXN erosion were successfully measured [28, 30]. The use of thicker coatings was not possible as the total thickness was limited by the ion beam energy available at the IFPN facility with the capability for handling whole Be tiles contaminated with tritium. However, this means that alternative mechanical methods of measurement such as surface profiling can be used in determining Be erosion rates. The choice of interlayer material is also important. In this case Ni was used which made the subsequent analysis of Ni as an impurity in deposits more complicated. A dissimilar element not used elsewhere in JET would have been a better choice. The results of the study show that the availability of facilities and choice of coating thickness and interlayer material will be limiting factors for marker coating studies where samples are to be located in high erosion areas and exposed over long periods of time.

Acknowledgments

ORCID iDs

A Widdowson ⓘ https://orcid.org/0000-0002-6805-8853
S Aleiferis ⓘ https://orcid.org/0000-0001-7529-470X
E Alves ⓘ https://orcid.org/0000-0003-0633-8937
L Avotina ⓘ https://orcid.org/0000-0001-5197-4196
A Baron-Wiechec ⓘ https://orcid.org/0000-0001-9458-6679
N Catarino ⓘ https://orcid.org/0000-0003-3879-1533
V Corregidor ⓘ https://orcid.org/0000-0001-8323-0634
K Heinola ⓘ https://orcid.org/0000-0002-0601-8274
I Jepu ⓘ https://orcid.org/0000-0001-8567-3228
C Makepeace ⓘ https://orcid.org/0000-0002-4177-0787

References

[1] Matthews G F *et al* 2011 *Phys. Scr.* **T145** 014001
[2] Baron-Wiechec A *et al* 2015 *J. Nucl. Mater.* **463** 157–61
[3] Heinola K *et al* 2015 *J. Nucl. Mater.* **463** 961–5
[4] Heinola K *et al* 2016 *Phys. Scr.* **T167** 014075
[5] Baron-Wiechec A, Heinola K, Likonen J, Alves E, Catarino N, Coad J P, Corregidor V, Jepu I, Matthews G F, Widdowson A and (JET Contributors) 2018 *Fusion Eng. Des.* **133** 135–41
[6] Widdowson A *et al* 2014 *Phys. Scr.* **T159** 014010
[7] Rubel M *et al* 2017 *Nucl. Fusion* **57** 066027
[8] Barradas N P, Catarino N, Mateus R, Magalhães S, Alves E, Siketić Z, Bogdanović Radović I and Radović I B 2015 *Nucl. Instrum. Methods Phys. Res.* B **346** 21–5
[9] Catarino N, Barradas N P and Alves E 2016 *Nucl. Instrum. Methods Phys. Res.* B **371** 50–3
[10] Kuan H-M, Bonner T W and Risser J R 1964 *Nucl. Phys.* **51** 481–517
[11] Möller W and Besenbacher F 1980 *Nucl. Instrum. Methods* **168** 111–4
[12] Catarino N, Barradas N P, Corregidor V, Widdowson A, Baron-Wiechec A, Coad J P, Heinola K, Rubel M, Alves E and JET contributors 2017 *Nucl. Mater. Energy* **12** 559–63
[13] Rubel M *et al* 2013 *J. Nucl. Mater.* **438** S1204–7
[14] Widdowson A, Baldwin M J, Coad J P, Doerner R P, Hanna J, Hole D E, Matthews G F, Rubel M, Seraydarian R and Xu H 2009 *J. Nucl. Mater.* **390–391** 988–91
[15] Barradas N P and Jeynes C 2008 *Nucl. Instrum. Methods Phys. Res.* B **266** 1875–9
[16] Avotina L, Jepu I, Baron-Wiechec A, Kresina M, Widdowson A and JET contributors 2019 *Phys. Scr.* (https://doi.org/10.1088/1402-4896/ab3c38)
[17] Pajuste E, Kizane G, Vitins A, Igaune I, Avotina L, Zarins R and JET Contributors 2017 *Nucl. Mater. Energy* **12** 642–7
[18] Widdowson A *et al* 2017 *Nucl. Fusion* **57** 086045
[19] Likonen J *et al* 2019 *Nucl. Mater. Energy* **19** 166–78
[20] Jepu I *et al* 2019 *Nucl. Fusion* **59** 086009
[21] Pintsuk G, Brezinsek S, Huber A, Rubel M, Widdowson A and Conributors J E T 2019 *Phys. Scr.* (https://doi.org/10.1088/1402-4896/ab4d72)
[22] Bykov I, Bergsåker H, Possnert G, Heinola K, Miettunen J, Groth M, Petersson P, Widdowson A and Likonen J 2015 *J. Nucl. Mater.* **463** 773–6
[23] Bergsåker H *et al* 2014 *Nucl. Fusion* **54** 082004
[24] Widdowson A *et al* 2019 *Nucl. Mater. Energy* **19** 218–24
[25] Arnoux G *et al* 2014 *Phys. Scr.* **159** 14009
[26] Brezinsek S *et al* 2015 *Nucl. Fusion* **55** 063021
[27] Romazanov J *et al* 2019 *Nucl. Mater. Energy* **18** 331–8
[28] Krat S, Mayer M, Bykov I, Lungu C P, de Saint A G, Widdowson A, Carvalho I S and JET Contributors 2017 *Nucl. Mater. Energy* **11** 20–4
[29] Widdowson A *et al* 2016 *Phys. Scr.* **T167** 014057
[30] Krat S, Gasparyan Y, Pisarev A, Bykov I, Mayer M, de Saint Aubin G, Balden M, Lungu C P, Widdowson A and JET-EFDA contributors 2015 *J. Nucl. Mater.* **456** 106–10